Journal of the Korean Physical Society, Vol. 40, No. 5, May 2002, pp. 942∼945 Brief Reports

# Characterization of Large-Area Inductively Coupled Plasma by Use of a Long-Range Fast-Scanning Probe

Yong Ho Jung,* Yong-Sup Choi and Kyu-Sun Chung
*Department of Nuclear Engineering, Hanyang University, Seoul 133-791*

Jun-Kyo Bak
*Device Development Division, Korea Basic Science Institute, Daejon 305-333*

(Received 4 March 2002)

Spatial variations of plasma parameters were measured in a large, inductively coupled plasma (ICP) chamber (diameter: 610 mm) by using a fast scanning probe (FSP), which could scan a length of 100 cm at a speed of 0.8 m/sec. The plasma parameters were measured by using single, triple, and emissive probes installed at the tip of FSP. A new modified diffusion model was introduced to analyze the spatial variations of the normalized density since the variable mobility model cannot explain the current measured data. Inclusion of ion thermal motion gives more reasonable results than the variable mobility model.

PACS numbers: 52.70.Ds, 51.50.+v, 52.55.Jd
Keywords: Inductive coupled plasma, Hanbit, Fast-scanning probe, Variable mobility model, Combined mobility model

Inductively coupled plasma (ICP) sources have been recognized as major candidates to meet the demand for large plasma sources in the plasma-aided manufacturing industry [1–3]. Various numerical models for and experiments on ICP characterization have been tried to understand the basic mechanism of ICP. If a large-area plasma source is to be characterized with an electric probe, smaller and faster devices becomes preferable to avoid unnecessary disturbances of the plasma. A long-range fast-scanning probe (FSP) was developed to measure the large-area plasma in the plug region of the "Hanbit" device [4], which is a large Tandam mirror device in the Korea Basic Science Institute. This FSP was tested in a RF test facility (RFTF) device before attaching it to the "Hanbit" magnetic mirror device. This paper addresses the measured plasma density profiles of on RFTF device generating a large plasma with a diameter of 60 cm.

The scheme of the experimental device is shown in Fig. 1. The RFTF device has a double half-turn antenna, which has a diameter of 380 mm, and a pair of circular limiters, which have diameters of 350 mm. Plasmas were generated by using 4-MHz RF with a power of 100∼600 W. Helium gas was used in the experiment. The plasma parameters were measured with single, triple, and emissive probes along the radial direction and the FSP was installed 280 mm apart from the antenna along the axial direction. Single probe (SP) and triple probe (TP) measurements were made using 1-mm-diameter, 4.3-mm-long molybdenum wire. The triple probe was insulated by using a 6-mm-diameter, 4-hole ceramic tube. To avoid the breakage due to impact of the scanning motion, we used 1 % thoriated tungsten with a 10-mil diameter as the tip of the emissive probe (EP), instead of using 1-mil tip. Due to the thick tungsten tip, the possibility of severe perturbation of the plasma had been raised,

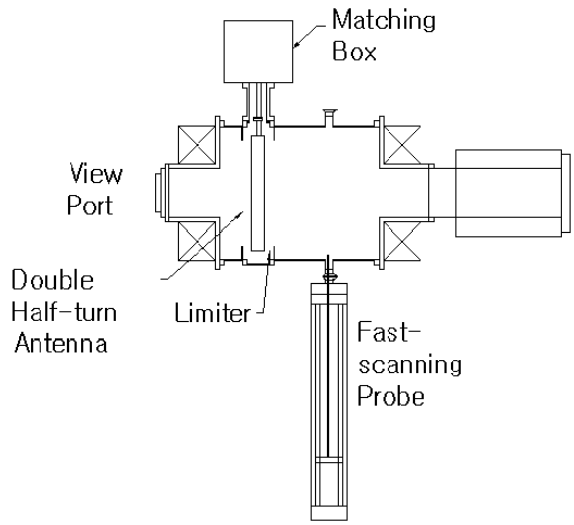


Fig. 1. Experimental apparatus.

*E-mail: yhjung@ihanyang.ac.kr

but a comparison between the measurement results for the 1-mil tip and for the 10-mil tip showed nearly the same value of the plasma potential within the error of 0.1 eV. In this experiment, a strong emission method was applied to get the plasma potential ($V_p$). When the temperature of the probe surface is sufficiently high, the floating potential of an emissive probe becomes close to plasma potential [5]. To reduce RF-noise, a low-pass filter with a 1-MHz cut-off frequency was used during all the experiments.

The radial variations in the electron temperature ($T_e$) and the density ($n_e$) were $T_e$=3.5∼4.5 eV and $n_e$=5×10$^9$∼3×10$^{10}$ cm$^{-3}$ at a pressure of $P$=4∼23 mTorr. As the pressure increases, the density increases while the temperature decreases. Except near the wall, the electron temperature is uniform in the radial direction, regardless of pressure. The plasma ($V_p$) and the floating potential ($V_f$) are measured by using an emissive probe, and the electron temperature is deduced from the following relation [5]:

$$T_e = \frac{e(V_p - V_f)}{3.34 + 0.5\ln(\mu)}, \tag{1}$$

where $\mu$ is the mass number of the ions, the electrons are assumed to be isothermal, and the sheath and the probe area is treated as same. There is some difference between the electron temperatures measured by EP and TP while the electron temperature measured by SP and TP seem to be almost the same in the central region. This may be due to the following reasons: (a) the ratio of sheath and probe area ($A_s/A_p$) being neglected, (b) the strong electron emission in the low-density area, (c) violation of isothermal properties due to atomic processes. For the first case, if we add sheath area effect, then the Eq. (1) should be written as

$$T_e = \frac{e(V_p - V_f)}{3.34 + 0.5\ln(\mu) + \ln(A_s/A_p)}. \tag{2}$$

Depending upon the sheath thickness ($\chi_s$), $\ln(A_s/A_p)$ can vary as 0.3∼1.5 for $n_e$=10$^{10}$ cm$^{-3}$ ($\chi_s$=1∼10$\lambda_D$), so that $T_e$ can have different values by 10∼40 %. As for the second case, when a strongly emitting probe was inserted, the emitted electron density may be similar or greater than that of the plasma at the surface region of chamber. For example, if the tungsten is heated up to 2400 K, the emitted current will be 234 A/cm$^2$ according to Dushman and Ewald [6]. As the surface area of the emissive probe is about 0.1 cm$^2$, if the electron is emitted with 0.2 eV energy; then, 5.6×10$^{13}$ electrons will be emitted per second.

As the probe was moved into the central region, the perturbative effect of the emissive probe decreased due to the increased plasma density. Anyway, through all radial direction, the emissive probe show results higher value than those from triple or single probes. Also, Fig. 2 shows a comparison of the single probe measurement with TP and EP. Similar values are seen with TP and EP.

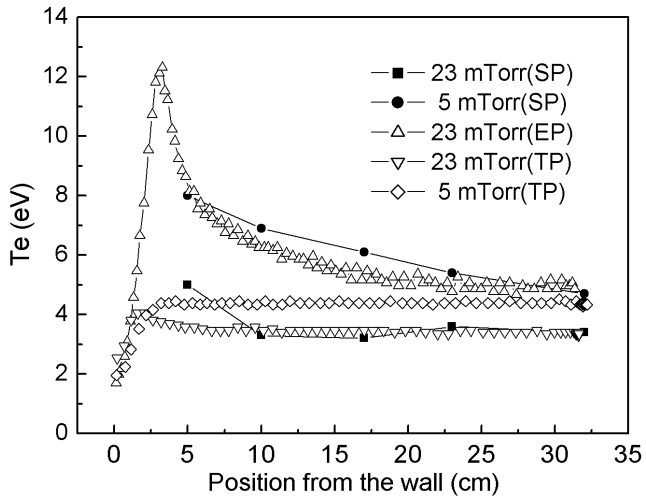


Fig. 2. Comparison of the measured $T_e$ results for SP, TP and EP.

From these results, the spatial distributions of $T_e$, $n_e$, $V_f$, and $V_p$ can be obtained. Using the results, the normalized density profile of the cylindrical chamber was investigated. For the first time, a variable mobility model [7] was applied to analyze the normalized density profile. Although the analytical solution for this model was given by Godyak [8], his solution was only a parallel plane geometry. That model was redefined here for cylindrical geometry. According to the variable mobility model (VMM) for a cylindrical geometry, the normalized density profile in a cylindrical chamber can be given from the continuity equation with a dimensionless variable as the following:

$$\frac{1}{x}\frac{d}{dx}\left(x\left(-y\frac{dy}{dx}\right)^{1/2}\right) = \alpha y, \tag{3}$$

where $y = n/n_0$, $x = r/a$, and $\alpha = \nu_{iz}\sqrt{\pi M a^3/2\lambda_i T_e}$. $n$ is the plasma density, $n_0$ is the plasma density at the center, $\nu_{iz}$ is the ionization frequency, $M$ is the mass of the ion, $a$ is the chamber radius, $\lambda_i$ is the ion mean free path, and $T_e$ [eV] is the electron temperature.

Although the above equation is difficult to solve analytically, its numerical solution can be easily given by integrating Eq. (3) with boundary conditions of $y$=1 and $dy/dx$=0 at $x$=0. Then, it can be easily solved with a finite different method:

$$y(i+1) = \left[y(i)^2 - 2\frac{\alpha^2\delta}{x(i)^2}\left\{\sum_{k=0}^{i} x(k)y(k)\delta\right\}^2\right]^{1/2}, \tag{4}$$

where "$i$" indicate the mesh number of position ($x$) and density ($y$) and $\delta$ is the size of the spatial mesh. From this relation, all $y(i)$ values can be determined if the $y(0)$ and the $y(1)$ values are given. The value of $y(0)$ is known, and $y(1)$ can be acquired by limit as follows: $y(1) = [y(0)^2 - 2\alpha^2\delta^3]^{1/2}$.

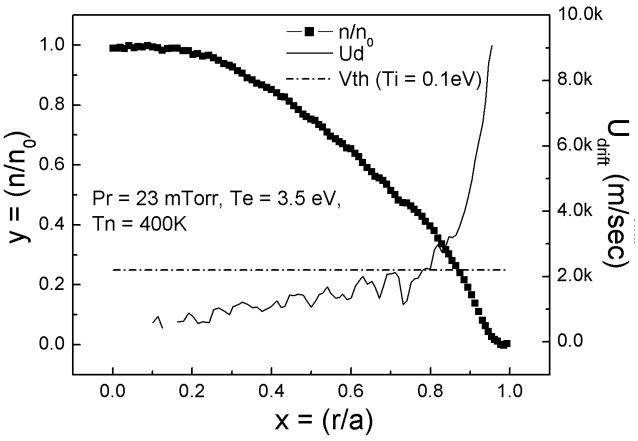


Fig. 3. Comparison of $v_{thermal}$ and $v_{drift}$.

Application of Eq. (4) to our experimental data cannot produce good results, although the experiment has been done at low pressure (5∼23 mTorr). That can be explained by the following reason: thermal velocity of the ions is not included in the VMM. In this experiment, the drift velocity of the ions was not much faster than the thermal velocity, as assumed by the variable mobility model. A comparison of these velocities is shown in Fig. 3. If diffusion due to the thermal velocity is to be combined with the drift velocity, a drift-Maxwellian ion distribution function must be assumed, and an average ion-neutral collision frequencys is calculated. Using that collision frequency, the continuity equation can be solved. To include the thermal velocity effect, we did not neglected the ion temperature, and we used the electron assumption as in the previous model; *i.e.*, the electron thermal velocity is much larger than the drift velocity. With that assumption, the continuity equation can be written as

$$\nabla \cdot \Gamma = \nabla \cdot \left( -\frac{kT_e(1+\gamma)}{M\nu_m} \nabla n \right) = \nu_{iz} m, \tag{5}$$

where $\gamma$ is the ratio $T_i/T_e$ and $\nu_m$ is the momentum collision frequency. If this equation is to be solved, the ion-neutral collision frequency must be recalculated with respect to the drift and the thermal velocities of the ions. The radial direction component of Eq. (5) can be integrated over $x$ in cylindrical geometry with dimensionless variables:

$$\frac{dy}{dx} = -\frac{m\nu_m}{k(T_e+T_i)} \frac{1}{x} \int_0^x a^2 \nu_{iz} y x' dx'. \tag{6}$$

From the flux equation, the drift velocity can be written as

$$u = -\frac{k(T_e+T_i)}{m\nu_m} \frac{1}{ay} \frac{dy}{dx} = \frac{a\nu_{iz}}{yx} \int_0^x y x' dx'. \tag{7}$$

Using a finite difference method, we can rewrite Eqs. (6) and (7) as

$$y(i+1) = y(i) - \frac{\beta \delta \nu_m}{x(i)} \sum_{k=0}^{i} y(k) x(k) \delta, \tag{8}$$

where $\beta = \frac{ma^2\nu_{iz}}{k(T_e+T_i)}$, and $u(i) = \frac{a\nu_{iz}}{y(i)x(i)} \sum_{k=0}^{i} y(k)x(k)\delta$. Initial values are given as $u(0) = 0$, $y(0) = 1$, $u(1) = a\delta\nu_{iz}$, and $y(1) = 1 - \beta\delta^2\nu_m$.

When the pressure decreases or the neutral gas temperature increases, the density profile tends to be flat. Because the neutral gas temperature determines the number density of neutral particles, it has a deep relation with the ionization frequency, the momentum collision frequency, and the density profile. Usually, the temperature of the neutral gas is reported as 300∼500 K [9,10]. As shown in Fig. 4, a small difference in the neutral par-

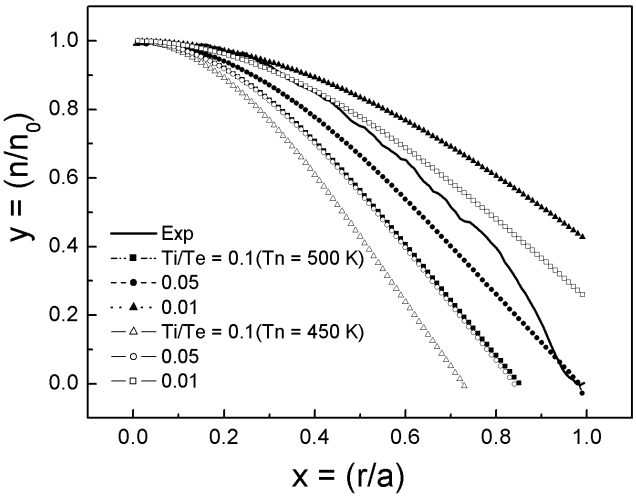


Fig. 4. Effect of the neutral and the ion temperature on the density profile.

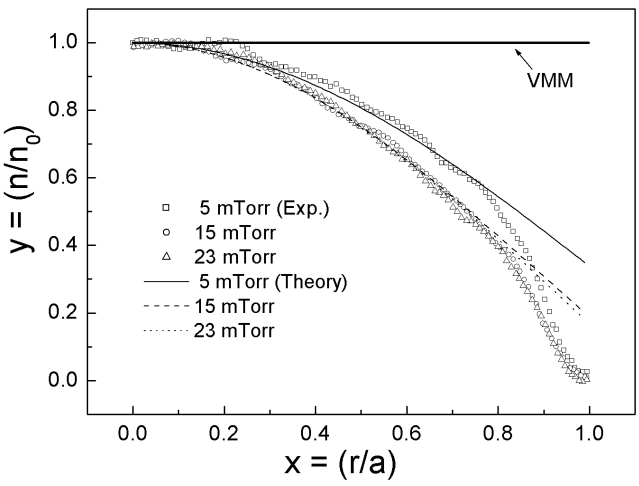


Fig. 5. Comparison of the experimental results with the simulation.

ticle temperature, such as measurement error, can cause a big difference in the density profile. However, not many reports exist on measuring the neutral gas temperature in plasmas, and reported results have relatively big measurement errors, as much as 50 K [9]. Figure 5 shows a comparison of the experimental results with the results from the variable mobility and combined diffusion models.

In summary we developed a new model to analyze the normalized density profile of large inductively coupled plasma, which include effect of ion thermal motion, which has been neglected in VMM. Thermal velocity of ion and neutral temperature seems to play an important role in determining of spatial density profile. Although combined mobility model (CMM) cannot fit the density profile of edge region of plasma, it gives better fitting the data than by VMM. Discrepancy between the theory and experiment near the wall would be explained by including spatial temperature variation and atomic process such as surface recombination.

## ACKNOWLEDGMENTS

This work was supported by the Korea Basic Science Institute and by the Brain Korea 21 project.

## REFERENCES

[1] J. Hopwood, Plasma Sources Sci. Technol. **1**, 109 (1992).
[2] J. S. Kim, G. H. Kim, T. H. Chung, G. Y. Yoem and K. H. Kwon, J. Korean Phys. Soc. **38**, 259 (2001).
[3] S. H. Won, J. H. Youn, T. Jang and B. Y. Moon, J. Korean Phys. Soc. **39**, 123 (2001).
[4] S. M. Hwang, G. S. Lee, J. G. Yang, K. K. Choh, J. H. Choi, J. W. Choi, K. S. Chung, C. J. Dhoh, J. Hong, B. C. Kim, D. E. Kim, W. C. Kim, H. K. Lee, S. G. Lee, H. K. Na, Y. K. Oh, H. L. Yang, S. J. Yoo, N. S. Yoon, K. I. You and D. I. Choi, Fusion Technol. **35**, 99 (1999).
[5] N. Herskowitz, in *Plasma Diagnostics*, edited by O. Auciello and D. L. Flamm (Academic Press, New York, 1989), p. 113.
[6] S. Dushman and J. W. Ewald, Gen. Electric Rev. **26**, 154 (1923).
[7] M. A. Lieberman and A. J. Lichtenberg, *Principles of Plasma Discharges and Materials Processing* (John Wiley & Sons, New York, 1994), p. 137.
[8] V. A. Godyak, *Soviet Radio Frequency Discharge Research* (Delphic Associates, Falls Church, 1986).
[9] T. Hori, M. D. Bowden, K. Uchino and K. Muraoka, J. Vac. Sci. Technol. A **14**, 144 (1996).
[10] T. Nakano, H. Ohtake and S. Samukawa, Jpn. J. Appl. Phys. **35**, 338 (1996).